EphB3 signaling propagates synaptic dysfunction in the traumatic injured brain

HHS Public Access

Author manuscript

Neurobiol Dis. Author manuscript; available in PMC 2017 October 31.

Published in final edited form as:

Neurobiol Dis. 2016 October ; 94: 73–84. doi:10.1016/j.nbd.2016.06.007.

EphB3 signaling propagates synaptic dysfunction in the traumatic injured brain

Enmanuel J. Perez[a], **Maria L. Cepero**[a], **Sebastian U. Perez**[a], **Joseph T. Coyle**[c], **Thomas J. Sick**[b], and **Daniel J. Liebl**[a,*]

[a]The Miami Project to Cure Paralysis, Department of Neurosurgery, University of Miami Miller School of Medicine, Miami, FL, USA

[b]Department of Neurology, University of Miami Miller School of Medicine, Miami, FL, USA

[c]Harvard Medical School, Department of Psychiatry, McLean Hospital, Boston, MA 02115, USA

Abstract

Traumatic brain injury (TBI), ranging from mild concussion to severe penetrating wounds, can involve brain regions that contain damaged or lost synapses in the absence of neuronal death. These affected regions significantly contribute to sensory, motor and/or cognitive deficits. Thus, studying the mechanisms responsible for synaptic instability and dysfunction is important for protecting the nervous system from the consequences of progressive TBI. Our controlled cortical impact (CCI) injury produces ~20% loss of synapses and mild changes in synaptic protein levels in the CA3-CA1 hippocampus without neuronal losses. These synaptic changes are associated with functional deficits, indicated by > 50% loss in synaptic plasticity and impaired learning behavior. We show that the receptor tyrosine kinase EphB3 participates in CCI injury-induced synaptic damage, where EphB3$^{-/-}$ mice show preserved long-term potentiation and hippocampal-dependent learning behavior as compared with wild type (WT) injured mice. Improved synaptic function in the absence of EphB3 results from attenuation in CCI injury-induced synaptic losses and reduced D-serine levels compared with WT injured mice. Together, these findings suggest that EphB3 signaling plays a deleterious role in synaptic stability and plasticity after TBI.

Keywords

EphB3 receptors; D-serine; Synapse damage; Synaptic plasticity; Traumatic brain injury

1. Introduction

Every year millions of people suffer the devastating consequences of a traumatic brain injury (TBI) (Centers for Disease Control and Prevention (CDC), 2013; Hyder et al., 2007). TBI is

*Corresponding author at: The Miami Project to Cure Paralysis, The University of Miami, 1095 NW 14th Terrace, R-48, Miami, FL 33136, USA. dliebl@miami.edu (D.J. Liebl).

Supplementary data to this article can be found online at http://dx.doi.org/10.1016/j.nbd.2016.06.007.

Conflicts of interest

The authors declare no competing financial interests.

a complex disorder that leads to profound deficits in neurological function as a result of progressive pathological events. TBI can be categorized as an open or closed head injury ranging from mild to severe pathology. At the site of impact, moderate to severe brain injuries usually include vascular damage, cell loss, axonal and synaptic damage; however, synaptic dysfunction in the absence of cell loss has also been observed in more distal regions (Kotapka et al., 1991; Lowenstein et al., 1992). Moreover, synaptic damage is thought to be a major contributor to chronic neurological symptoms following mild concussive injuries (Harish et al., 2015; Merlo et al., 2014). For this reason, it is important to understand the mechanisms that regulate synaptic stability and plasticity in the traumatic injured brain.

Learning and memory deficits are commonly observed impairments following TBI (Lyeth et al., 1990; Schwarzbach et al., 2006; Witgen et al., 2005). Consolidation of short- and long-term memory is attributed to activity-dependent changes in synaptic strength (i.e. synaptic plasticity) in the hippocampus. NMDAR activation is critical for synaptic plasticity, as its activation is known to regulate glutamatergic receptor density in the post-synaptic membrane, bouton size, and synaptic strength (Adams et al., 2001; Hardingham and Bading, 2010; Hunt and Castillo, 2012). Recently, D-serine has been shown to function as the endogenous co-agonist for NMDARs, and together with glutamate is essential for synaptic plasticity, learning and memory (Balu et al., 2014; Han et al., 2015; Mothet et al., 2000; Wolosker et al., 1999a). D-serine is synthesized through the racemization of L-serine by the enzyme serine racemase (Wolosker et al., 1999b), though the mechanisms that regulate D-serine conversion and release after TBI have yet to be explored. What is known is that excessive activation of NMDARs is thought to play a key role in TBI pathology, and underlies excitotoxic cell death (Faden et al., 1989; Hardingham et al., 2002). It is less clear whether sub-excitotoxic activation of NMDAR by D-serine after TBI can lead to synaptic damage.

Receptor tyrosine kinases are also associated with synaptic membranes and play important roles in regulating synaptic formation and function. In particular, Eph receptors (Ephs) have been shown to stabilize post-synaptic densities, regulate excitatory synaptic numbers, glutamate receptor transport, and synaptic plasticity (Antion et al., 2010; Grunwald et al., 2004; Henkemeyer et al., 2003; Hruska et al., 2015; Rodenas-Ruano et al., 2006). Both Ephs and their ligands (i.e. ephrins) are membrane bound and can elicit bidirectional signals upon interactions of pre- and post-synaptic membranes (Aoto and Chen, 2007; Klein, 2009; Pasquale, 2008). Astrocytes can also interact with neuronal components of the synapse in what is known as the tripartite synapse to regulate synapse formation and plasticity (Halassa et al., 2007; Perea et al., 2009). Astroglial release of glutamate and D-serine can alter synaptic function, where gliotransmitter levels in the synapse can fine-tune excitatory postsynaptic potentials (Araque et al., 2014; Gundersen et al., 2015; Halassa et al., 2007). Moreover, ephrinB3 interaction with EphB3 and EphA4 in astrocytes is known to influence hippocampal synaptic plasticity through regulation of D-serine synthesis and release (Zhuang et al., 2010). It is therefore important to understand the role of Eph-mediated signaling events following TBI, specifically the contribution to D-serine release and synaptic function.

Our findings suggest that elevated levels of D-serine after TBI may contribute to progressive CNS pathology. We also show that EphB3 negatively regulates excitatory glutamatergic

synaptic stability and plasticity after moderate TBI, as observed by decreased D-serine levels, improved synaptic stability and enhanced long-term potentiation in the absence of EphB3.

2. Materials & methods

2.1. Animals

EphB3 knockout (EphB3$^{-/-}$) mutant mice were bred on a C57Bl/6 background as previously described (Henkemeyer et al., 1996; Orioli et al., 1996). All procedures were performed on both wild type (WT) and EphB3$^{-/-}$ male mice 2–4 months of age and approved by the University of Miami Institutional Animal Care and Use Committee.

2.2. Controlled cortical impact (CCI) injury

Mice were initially anesthetized with a ketamine/xylazine cocktail and placed on a heating pad. Mice were placed in a stereotaxic frame, where they remained until the end of the procedure. The head was shaved and the skull was exposed through a skin incision. A 5 mm craniotomy was made over the right parieto-temporal cortex without disturbing the dura, with the epicenter coordinates at bregma: −2.0 mm; lateral: −2.5 mm. Mice were then subjected to a moderate CCI at a velocity of 4 m/s, 0.50 mm depth and 150 ms duration using an eCCI-6.0 device (Custom Design & Fabrication, Richmond, VA). The CCI consists of a pressurized metal piston delivering a blow at the aforementioned parameters directly onto the dura of the brain producing mechanical strain forces similar to those observed in human TBI (Osier et al., 2015). Following the impact, the skin was closed using 5-0 Vicryl synthetic absorbent sutures, and animals were placed into a clean cage on a heating pad until recovery from anesthesia. Mice received 0.9% saline and analgesic (Buprenorphine) injections and monitored bi-daily for one week.

2.3. Stereological cell and neuronal counts

Mice were anesthetized and perfused with 0.1 M phosphate buffer and 4% paraformaldehyde (PFA). Brains were dissected and serially cryo-sectioned (Leica CM 1900, Leica Biosystems Inc., Buffalo Grove, IL) at 15 μm/section from bregma −1.4 to −2.2 for a total tissue thickness ~1500 μm. For total hippocampal cell counts and regional volumetric analysis, hematoxylin and eosin staining was performed on serial sections. Micro Bright Field StereoInvestigator software package (MBF Bioscience, Williston, VT) was used to contour the dentate gyrus, hilus, CA3 and CA1 areas at 10× magnification. After contouring, a grid of 100 × 100 μm^2 was placed over each region of interest and hematoxylin-stained nuclei within a random sampling box of 50 × 50 μm^2 was counted using the optical fractionator at 63 × magnification for unbiased determination of cell number. Investigators were blind to experimental group. For neuronal counts, neuronal labeling with NeuN antibody (Cell Signaling, Beverly, MA) and DAPI was performed on serial sections. Randomized images of each hippocampal region were acquired at 40 × magnification using an Olympus BX50 microscope. ImageJ software was utilized to quantify DAPI-positive and NeuN-positive cells within the dentate granule cell, CA1 and CA3 pyramidal cell layers. Investigators were blind to experimental group.

2.4. Transmission electron microscopy (TEM)

Mice were anesthetized and perfused with 2% PFA/2% glutaraldehyde in 0.1 M phosphate buffer. Brains were dissected, embedded in chicken albumin agar and cut into 500 μm sections using a motorized vibrating-blade microtome (Leica VT1000s, Leica Biosystems Inc., Buffalo Grove, IL). CA1 hippocampal regions were dissected, cut into 1 mm^2 pieces, and further post-fixed with 3% EM grade glutaraldehyde. Ultrathin tissue sections were stained with conventional osmium-uranium-lead method containing 1% ethanolic phosphotungstic acid (EPTA). The CA1 hippocampus was visualized using a Philips CM-10 TEM operating at 80 kV. Sections were placed on a grid and non-overlapping randomized photographs (>20/section) were taken throughout the entirety of CA1 stratum radiatum. Photographs were digitized, and an investigator blinded to experimental group quantified synapses manually. The inclusion criteria for excitatory synapses included the presence of pre- and post-synaptic membranes with a discernible synaptic cleft, presence of asymmetric pre- and post-synaptic densities, and presence of synaptic vesicles at the presynaptic terminal as described previously (DeFelipe et al., 1999; Mayhew, 1996). Pre- and post-synaptic densities from quantified synapses were measured for synaptic area and length using ImageJ.

2.5. Western blot analyses

Ipsilateral hippocampal tissues from sham and CCI injured mice were homogenized in RIPA buffer with protease and phosphatase inhibitor cocktail (Sigma-Aldrich, St. Louis, MO) and benzonase nuclease (Millipore Corporation, Billerica, MA) and mixed by rocking at 4 °C for at least 15 min. Tissues were centrifuged, supernatant was recovered, samples were diluted and standardized to protein concentrations. Protein samples were separated on 8–10% SDS-PAGE gel and transferred to a nitrocellulose membrane. Membranes were then blocked with 5% milk or 5% BSA in 0.1 M phosphate buffer with 0.1% Tween-20 for 1 h at room temperature (RT) and incubated overnight at 4 °C with primary antibodies. Membranes were incubated for 1 h at RT with HRP-conjugated secondary antibodies (Jackson Immunoresearch Laboratories, West Grove, PA). Bands were visualized using SuperSignal substrate (ThermoScientific, Pittsburg, PA). The following primary antibodies were used: anti-GluR1, anti-NR1, anti-NR2B (EMD Millipore, Billerica, MA), anti-GFAP (BD Biosciences, San Jose, CA), anti-SNAP25, anti-SNAP23 (ABCAM, Cambridge, MA) and anti-β-tubulin (Sigma-Aldrich, St. Louis, MO) antibodies. ImageJ was used to perform density analysis. Protein measurements were standardized to β-tubulin and normalized to average WT sham signals.

2.6. Intra-hippocampal infusion of ephrinB3

Alzet pumps (1003D, Alzet, Cupertino, CA) were preloaded with 112 μg/kg/day pre-clustered ephrinB3-Fc or Fc-only, while other experiments used 840 μg/kg/day D-serine or vehicle. Briefly, loaded pumps were connected to a brain infusion catheter and placed in 0.1 M phosphate buffer at 37 °C overnight (Theus et al., 2014). After the CCI injury, the infusion device was attached to the stereotactic holder and the tip of the cannula was lowered 1.7 or 2.0 mm into the hippocampus or lateral ventricle, respectively. The infusion device was secured to the skull using Loctite 454 prism gel (Henkel Corp. Rocky Hill, CT).

The pump was then placed under the skin in the back of the neck and the incision was closed with suture. Mice were placed in clean heated cages to recover.

2.7. Chemiluminescent assay

Mice were anesthetized and the ipsilateral hippocampi were immediately dissected and homogenized in RIPA buffer with protease and phosphatase inhibitor cocktail and benzonase nuclease and incubated by rocking at 4 °C for at least 15 min. Tissues were centrifuged, supernatants were recovered, and samples were diluted and standardized to protein concentrations. D-serine was measured by a chemiluminescent assay as previously described (Wolosker et al., 1999b; Zhuang et al., 2010). A 10 μl sample was mixed with 100 μl of medium containing 100 mM Tris-HCl, pH 8.8, 20 units/ml peroxidase, and 8 μM luminol. To decrease background signal of luminal, 10 μl of D-amino acid oxidase (DAAO) (75 units/ml) were added after a 15 min delay. Chemiluminescence kinetics was recorded for 4 min at RT with a FLUOstar Omega microplate reader (BMG Labtech, Ortenberg, Germany). The concentration of D-serine in each sample was compared to a standard curve. The linear range was 50–1000 pmol of D-serine in the sample and the detection limit was 30 pmol. Glutamate was measured using Amplex Red Glutamic Acid/Glutamate Oxidase Assay kit (Molecular Probes, Eugene, OR) following the manufacturer's protocol. Fluorescence was measured in a FLUOstar Omega microplate reader using excitation in the range of 530–560 nm and emission detection at 590 nm. To correct for background fluorescence, the values were subtracted from control well values (i.e. no glutamic acid).

2.8. Electrophysiology

2.8.1. In vivo electrophysiology—Mice were anesthetized with urethane (1.5 g/kg) and placed on a stereotaxic frame. A 25 μm concentric platinum-iridium bipolar stimulation electrode and platinum-iridium recording electrode were inserted through a craniotomy site at bregma: −2.0 mm; lateral: −2.0 mm; depth: 1.4 mm (stimulation electrode) and bregma: −1.8 mm; lateral: −1.4 mm; depth: −1 to −1.5 mm (recording electrode). Concentric platinum-iridium bipolar stimulation electrodes (tip diameter 25 μm, FHC, Bowdoin, ME) were placed in the Schaffer Collaterals and a recording glass micropipette filled with 150 mM sodium chloride (1–3 MΩ) was placed in the CA1 stratum radiatum. Field potentials were recorded and converted to digital using an Axoclamp 2B amplifier, Axon Instruments Digidata 1322A analog-to-digital converter, and Clampex (Axon Instruments) software for data acquisition and analysis. Input-output (I/O) curves were generated by delivering electrical monophasic pulses to the CA3 Schaffer Collaterals from a Grass S88 stimulator and S1U5 stimulus isolation unit, and measuring the field-excitatory post-synaptic potential (fEPSP) at increasing stimulus intensities. Stimulus intensities were then adjusted to give fEPSP amplitude at 45–55% of the maximum. A stable baseline fEPSP slope was recorded at a rate of 1/60 s for at least 30 min. A paired-pulse facilitation protocol was run using inter-pulse intervals of 20 ms, 40 ms, and 80 ms. Long term potentiation (LTP) was induced with high-frequency stimulation (HFS, 2 × 100 Hz, 1 s trains, 20 s inter-train interval). Post-HFS fEPSPs were recorded for at least 60 min. Post-tetanus fEPSP slopes were expressed as a percentage of the average fEPSP slope from the baseline recordings.

2.8.2. In vitro electrophysiology—Mice were anesthetized using isoflurane and decapitated. Brains rapidly removed, and to reduce tissue damage, were quickly immersed in oxygenated ice-cold fresh high sucrose containing artificial cerebrospinal fluid (high sucrose-aCSF): 100 mM sucrose, 60 mM NaCl, 3 mM KCl, 1.25 mM NaH_2PO_4, 28 mM $NaHCO_3$, 0.5 mM $CaCl_2$, 7 mM $MgCl_2$, 0.6 mM ascorbic acid, and 5 mM glucose equilibrated with 95% O_2:5% CO_2. Brains received a mid-sagittal hemisection and the ipsilateral hippocampi were carefully dissected from the overlying cortex. The hippocampi were mounted on agarose blocks, and cross-sectioned into 300 μm slices with a motorized vibrating-blade microtome (Leica VT1000s, Leica Biosystems Inc., Buffalo Grove, IL). Slices were gradually transferred from high sucrose-aCSF to a holding chamber containing 50% high sucrose-aCSF/50% aCSF. aCSF contained: 125 mM NaCl, 2.5 mM KCl, 1.25 mM NaH_2PO_4, 25 mM $NaHCO_3$, 2 mM $CaCl_2$, 1 mM $MgCl_2$, and 25 mM glucose, oxygenated with 95% O_2:5% CO_2 at RT. Slices were allowed to recover for at least 1 h in aCSF at RT before transfer to a submersion-type recording chamber perfused with aCSF oxygenated with 95% O_2:5% CO_2 at 32 °C. Field potentials were recorded using an Axoclamp 2B amplifier, Axon Instruments Digidata 1400 analog-to-digital converter, and Clampex software for data acquisition and analysis. The recording protocol was the same as used during in vivo electrophysiological recordings.

2.9. Fear conditioning test

The fear conditioning apparatus consists of a box (30 × 24 × 21 cm, Coulbourn Instruments, Whitehall, PA) with an electric grid floor (0.8 cm spacing, 4.8 mm diameter rods). Mice were placed in the box for habituation for 600 s. On the second day of the paradigm, mice were placed back in the box for 120 s followed by a 30 s tone (85 dB, 2 kHz) with a 0.7 mA foot shock delivered through the grid floor during the last 2 s of the tone. The animals remained in the box for an additional 60 s after the shock for a total duration of 210 s of training. At 24 h after training, mice were placed in the same box and freezing behavior was measured for 300 s to assess contextual fear conditioning. At 1 h after contextual fear assessment, cue fear conditioning was assessed by placing mice in a chamber with different wall coloration, lighting and scent and measuring freezing behavior for 360 s during which the tone (85 dB, 2 kHz) was delivered for the last 180 s. The box was cleaned with 70% EtOH and an enzymatic cleaner between animals. Freezing behavior was quantified using video-based analysis software (FreezeFrame, Coulbourn Instruments, Whitehall, PA).

2.10. Statistical analyses

Data were graphed using GraphPad Prism (GraphPad Inc., SanDiego, CA). Comparisons between WT sham and $EphB3^{-/-}$ sham, WT sham and WT CCI, or $EphB3^{-/-}$ sham and $EphB3^{-/-}$ CCI injured mice were measured. Student's two-tailed *t*-test was used for comparison of two experimental groups. One-way ANOVA or two-way ANOVA was used for comparison of more than two groups, followed by Bonferroni post-hoc correction. Kolmogorov-Smirnov (K-S) test was used to analyze the distribution of synaptic density areas and width in combination with Kruskal-Wallis test in the TEM studies. For hippocampal electrophysiological recordings two-way ANOVA and repeated measures ANOVA with Bonferroni post-hoc correction were used. Data is represented as mean value ± standard error of the mean (SEM).

3. Results

3.1. A CCI injury model to examine synaptic dysfunction without hippocampal neuronal loss

To examine the effects of traumatic brain injury (TBI) on synaptic stability and function, we took advantage of a well-described controlled cortical impact (CCI) injury model (Edward Dixon et al., 1991; Osier et al., 2015; Smith et al., 1995; Theus et al., 2014). While other TBI models exist, CCI injury allows for accurate replication of biomechanics similar to human TBI (Peña et al., 2005; Xiong et al., 2013; Zhang et al., 2014), and can be adapted to different injury severities depending on the experimental paradigm (BRODY et al., 2007; Chen et al., 2014; Saatman et al., 2006; Assis-Nascimento et al., 2016). To examine synaptic dysfunction in the TBI environment, we established a moderate mouse controlled cortical impact (CCI) injury model where hippocampal synaptic damage is independent of neuronal loss. Hematoxylin and eosin (H&E) stained CCI injured wild type (WT) tissues showed substantial cortical damage at 7 days post-CCI injury (dpi) as compared with sham controls (Fig. 1A, B); however, no overt hippocampal damage was observed (Fig. 1B) nor at 30 dpi (not shown). High magnification of CA1 pyramidal neurons (CA1) of the hippocampus in Thy-1-YFP reporter mice also showed no visible neuronal damage at 7 dpi (Fig. 1A', B'). Furthermore, significant upregulation in GFAP immunoreactivity was observed in the CA1 hippocampus after CCI injury but not in sham injured mice (Fig. 1C – D), which is consistent with activating hippocampal injury cascades that lead to hypertrophic astrocytes but no neuronal loss after brain injury (Burda et al., 2016; Chen et al., 2014; Laird et al., 2008).

To determine whether CCI injury affects synaptic function at 7 dpi, we measured CA3-CA1 hippocampal field excitatory post-synaptic potentials (fEPSPs) and long-term potentiation (LTP) in vivo. CCI injury led to a significant deficit in synaptic recruitment at higher stimulus intensities, as observed by a significant difference in the input/output (I/ O) curve at stimulus intensities of 20 and 30 μA between sham and CCI injured mice ($p = 0.0313$ and $p = 0.0162$, respectively; Fig. 1E). In addition, examination of LTP showed a significant reduction in the CA3-CA1 fEPSP slope in CCI injured mice ($p = 0.0132$) when compared with sham controls (Fig. 1F; n = 4–5/group). We next examined hippocampal-dependent learning and memory using a fear-conditioning paradigm known to detect deficits after TBI (Titus et al., 2013). No difference was observed in habituation and baseline training; however, WT sham mice displayed significant contextual and cued freezing behavior that was not observed in CCI injured mice ($p < 0.001$ and $p = 0.0287$, respectively; Fig. 1G; n = 7/group). Together, these findings demonstrate that CCI injury results in significant synaptic dysfunction and learning deficits even in the absence of gross hippocampal tissue damage.

To evaluate whether synaptic deficits are independent of hippocampal cell loss or atrophy, we quantified the number of CA1 pyramidal cells, CA3 pyramidal cells and dentate granule cells (DGC) at 7 dpi using non-biased stereology on hematoxylin stained (Fig. 1H; n = 5/ group) and anti-NeuN immunolabeled (Fig. 1I; n = 3/group) hippo-campal tissues in regions directly ventral to the injury epicenter. We also performed tissue volume analysis at 7 dpi between groups using non-biased stereology (SFig. 1A–D; n = 5/group). For all analyses, we

observed no significant difference in the number or volume of CA1 or CA3 pyramidal cells between sham and CCI injury. We did observe a modest increase in DGC numbers after CCI injury as compared with sham counterparts ($p = 0.0324$; Fig. 1H), but significant difference was not observed in the NeuN-positive cells (Fig. 1I), DGC or hilus volumes (SFig. 1C, D). Quantitative differences between hematoxylin and anti-NeuN counts likely reflect differences in cell identification as previously reported (Zhu et al., 2015), where hematoxylin counts where based on morphological criteria while anti-NeuN counts were based on nucleated anti-NeuN cell bodies. Together, these findings support a CCI injury model where the mechanisms of synaptic damage can be examined independent of neuronal death.

3.2. EphB3 levels are increased after CCI injury

EphB3 signaling is known to have a deleterious effect in tissue recovery (Theus et al., 2010, 2014); however, its effects on synaptic stability and function after CCI injury are still poorly defined. To evaluate the role of EphB3 in the injured hippocampus, we first examined EphB3 levels in the sham and CCI injured hippocampus at 3 and 7 dpi. Western blot analysis showed a significant increase in EphB3 levels at 3 and 7 dpi as compared with sham controls (Fig. 2A; n = 4/group), which correspond to the peak periods of synaptic dysfunction. In the absence of EphB3 (i.e. EphB3$^{-/-}$ mice)we observed reduced gross cortical damage at 7 dpi (Fig. 2C) as compared with WT CCI injury (Fig. 1B) and EphB3$^{-/-}$ sham (Fig. 2B) mice, which supports previous findings (Theus et al., 2014). In addition, no overt gross hippocampal damage was observed and stereological quantification of cell numbers showed no differences in CA1 and CA3 pyramidal cell layers (Fig. 2D) or regional hippocampal volumes between sham and CCI injured EphB3$^{-/-}$ mice (SFig. 1A–D; n = 5/group). In the injured EphB3$^{-/-}$ hippocampal dentate gyrus (Fig. 2D), we did observe an increase in DGC numbers ($p = 0.0324$) similar to that observed in WT mice after injury (Fig. 1H).

3.3. CCI injury leads to EphB3-dependent synaptic loss in the hippocampus

To begin evaluating hippocampal synaptic damage following CCI injury, we used transmission electron microscopy (TEM) to quantify synaptic numbers as well as measured pre- and post-synaptic densities in the ipsilateral CA1 stratum radiatum of WT and EphB3$^{-/-}$ mice at 7 dpi (Fig. 3; n = 4/group). Tissues were cut into ultrathin sections (Fig. 3A), the CA1 was dissected and a placed on a grid (Fig. 3B), and non-overlapping photographs of EPTA-stained CA1 stratum radiatum were taken (Fig. 3C). We then quantified asymmetric (i.e. excitatory) synapses (Mayhew, 1996; Sheng and Kim, 2011) if they met the following criteria: apposed pre- and post-synaptic densities, the presence of pre-synaptic vesicles and a visually discrete synaptic cleft (Fig. 3D, E). WT CCI injured mice showed a significant ~20% reduction ($p < 0.001$) in synaptic numbers compared with sham controls (Fig. 3F). We observed fewer synapses in EphB3$^{-/-}$ sham mice than WT sham mice ($p < 0.001$; Fig. 3F), suggesting that EphB3 may regulate synaptic formation or maintenance during development. For this reason, CCI injury values were only compared to sham controls of their respective genotype. Interestingly, we did not observe injury-induced synaptic losses in CCI injured EphB3$^{-/-}$ mice as compared to EphB3$^{-/-}$ sham controls (Fig. 3F).

In addition to overt synaptic loss in WT mice, CCI injury could also lead to disorganization of subsisting synapses, interruption of glutamatergic signaling scaffolds and impaired excitatory signaling (Carlson et al., 2015; Luo et al., 2011, 2014). Thus, we next quantified the average area of both pre- and post-synaptic density (SD) at 7 dpi in sham and CCI injured WT and EphB3$^{-/-}$ mice. We observed no significant difference in the area of pre-SD and post-SD between WT sham and CCI injured mice (Fig. 3G, H), suggesting that remaining synapses are possibly stabilized within the first week. We did observe a significant increase ($p < 0.001$) in the post-SD area in EphB3$^{-/-}$ sham mice compared with WT sham mice (Fig. 3G). However, in the hippocampus of EphB3$^{-/-}$ mice, CCI injury lead to significantly less ($p = 0.0023$) area covered by the post-SD protein network in the absence of synaptic loss (Fig. 3G), suggesting that EphB3 may play deleterious roles in synaptic maintenance after CCI injury.

To further evaluate synaptic densities, we examined the distribution of synaptic density size between groups (Fig. 3I, J). Post-SD areas showed a left-modal distribution that ranged from 0 to 11,000 nm^2 for sham-and CCI-injured WT and EphB3$^{-/-}$ synapses (Fig. 3I). The overall distribution of synaptic densities was evaluated using a Kolmogorov– Smirnov (KS) test, which showed significant variance between the distribution of WT versus EphB3$^{-/-}$ sham ($p < 0.001$) and between EphB3$^{-/-}$ sham versus EphB3$^{-/-}$ CCI injured post-SD areas ($p < 0.001$). However, no significant differences were observed between groups at any specific area using two-way repeated measures ANOVA. Pre-SD areas also showed a left-modal distribution ranging from 0 to 5400 nm^2 for sham- and CCI-injured WT and EphB3$^{-/-}$ synapses (Fig. 3J). KS tests did not show significant difference between sham groups or sham versus CCI injury within genotypes. These findings confirm that changes observed in pre- and post-SD areas (Fig. 3G – H) were due to a shift in the overall sizes of the synaptic densities.

We also evaluated the variability in spine size based on average post-SD diameters, which may differ from increased protein aggregation area (Martone et al., 1999). Examination of post-SD diameters showed no difference in average diameter between groups (Fig. 3K); however, analysis of cumulative distributions did show significant difference between groups using KS test. Specifically, we observed a significant difference between EphB3$^{-/-}$ sham versus EphB3$^{-/-}$ CCI injury ($p = 0.0053$). Two-way repeated measures ANOVA showed significant interactions between diameter and group, where the Bonferroni post-hoc test showed significant difference ($p < 0.01$) between EphB3$^{-/-}$ sham and EphB3$^{-/-}$ CCI injury at diameters ranging between 0.21 and 0.25 μm (SFig. 2A).

To better evaluate the synaptic unit, we next examined the relationship between post-SD and pre-SD areas (i.e. post-SD:pre-SD ratio), since a synchronous change in spine size is necessary for enhancements in synaptic strength (Meyer et al., 2014). We observed reversed trends between WT and EphB3$^{-/-}$ ratios after CCI injury, where WT ratios increased significantly ($p = 0.0084$) while EphB3$^{-/-}$ ratios reduced significantly ($p < 0.001$) (Fig. 3L – P). Examination of cumulative distributions showed group differences between WT sham versus EphB3$^{-/-}$ sham ($p = 0.0105$), WT sham versus WT CCI injury ($p = 0.0024$), and EphB3$^{-/-}$ sham versus EphB3$^{-/-}$ CCI injury ($p < 0.001$). Two-way repeated measures ANOVA of frequency distributions by ratio size showed no significant interaction between

ratio and group (SFig. 2B). These findings suggest that reduced synaptic function and behavioral deficits inWT CCI injured mice may be associated with overall synaptic loss as well as dysregulation of the synaptic unit within the remaining synapses.

3.4. Absence of EphB3 signaling improves synaptic plasticity after CCI injury

To determine whether synaptic function is affected by the EphB3-dependent ultrastructural changes after CCI injury, we examined CA3-CA1 hippocampal field excitatory postsynaptic potentials (fEPSPs) in vivo in the presence and absence of EphB3 (Fig. 4; n = 4–6/group). To assess basal synaptic transmission we recorded input-output (I/O) curves at increasing stimulus intensities, and observed no significant interaction among animal groups and stimulus intensities (Fig. 4A); however, we did observe significant differences in fEPSP slope at different stimulus intensities ($p < 0.0001$) and between animal groups ($p = 0.0132$). As we observed in our initial characterization of our CCI injury model, WT mice subjected to CCI injury exhibit a significant downward shift in the I/O curve at higher stimulus intensities. Conversely, when we measured the I/O curves in EphB3$^{-/-}$ mice, we observed no significant difference in synaptic recruitment after CCI injury compared to sham (Fig. 4A). Examination of paired pulse facilitation (PPF), a measure of presynaptic function, revealed no significant differences between animal groups (Fig. 4B). These findings are consistent with our in vitro hippocampal slice recordings (SFig. 3A) and corroborate our ultrastructural data that the effects observed after CCI injury are mainly post-synaptic in nature. Finally, examination of long-term potentiation (LTP) in vivo at the CA1 hippocampal synapse showed a significant interaction between animal group and time ($p < 0.0001$) and main effect for animal groups ($p = 0.0131$) and time ($p < 0.0001$) (Fig. 4C). Analysis of fEPSP slope post-HFS (high frequency stimulation) revealed significant reductions in both early and late LTP in WT CCI injured mice ($p = 0.0075$ and $p = 0.0064$, respectively) that were not observed in EphB3$^{-/-}$ CCI injured mice when compared to genotype-matched shams (Fig. 4C – E). Similarly, recordings from hippocampal slices harvested at 7 dpi from CCI injured WT mice showed reductions in fEPSP slope, but not in slices from CCI injured EphB3$^{-/-}$ mice (SFig. 3B – D). These findings support a deleterious role of EphB3 in synaptic function after CCI injury.

3.5. Absence of EphB3 signaling results in improved hippocampal learning after CCI injury

We next examined hippocampal-dependent learning and memory using a fear-conditioning paradigm. Following injury, WT and EphB3$^{-/-}$ mice were habituated at 5 dpi, trained at 6 dpi and tested for freezing behavior at 7 dpi. No significant differences were observed between sham and CCI or between genotypes during training periods (Fig. 5; n = 8–15/group). During the contextual testing period, we observed a main effect for animal groups ($p < 0.0001$). CCI injury led to a significant ($p < 0.0001$)~50% reduction in contextual and cued freezing behavior in WT CCI injured mice when compared with WT sham mice. Contrarily, EphB3$^{-/-}$ CCI injured mice performed statistically similar to sham controls in both contextual and cued learning paradigms, although a trend towards reduced performance after injury was observed, possibly due to extra-hippocampal damage following CCI injury. These findings support our electrophysiological recordings that suggest activation of EphB3 may exacerbate injury-induced deficits in hippocampal function.

3.6. EphB3 does not affect injury-induced changes in hippocampal synaptic proteins

To investigate the molecular basis of the changes in synaptic plasticity observed in CCI-injured hippocampal neurons in the presence and absence of EphB3, we examined the expression of key synaptic proteins essential for excitatory synaptic transmission. Specifically, we quantified protein levels for post-synaptic glutamatergic receptor subunits (i.e. GluR1, NR1 and NR2B) and synaptosomal-associated protein-23 (SNAP23) and −25 (SNAP25) in sham and CCI injured whole hippocampal tissues at 7 dpi using Western blot analysis (Fig. 6; n = 4/group). We observed stable levels of the AMPAR subunit GluR1 regardless of genotype or injury state (Fig. 6A). The NMDAR subunits NR1 and NR2B contribute to hippocampal learning and memory as well as injury-induced excitotoxicity (Gambrill and Barria, 2011; Paoletti et al., 2013). NR1 subunits, the site for D-serine binding, showed no significant differences from sham controls for either genotype (Fig. 6B). In WT mice we observed a significant increase in NR2B levels after CCI injury ($p = 0.0293$) that was also observed in EphB3$^{-/-}$ mice as compared with their respective sham controls ($p = 0.0159$) (Fig. 6C). We also examined SNARE complex proteins, SNAP-25 and SNAP-23, involved in neuronal and astrocytic vesicular release, respectively. We did not observe significant differences in SNAP-25 nor SNAP-23 levels after CCI injury for either WT or EphB3$^{-/-}$ mice (Fig. 6D, E). Finally, since increased glial fibrillary acidic protein (GFAP) levels are a hallmark of reactive astroctyes after brain injury, we examined whether WT and EphB3$^{-/-}$ mice showed differences in GFAP expression at 7 dpi. Similar increases in GFAP immunoreactivity were observed between WT ($p = 0.0003$) and EphB3$^{-/-}$ ($p = 0.0002$) mice (Fig. 6F). Together, these findings suggest that significant variances in core synaptic proteins do not underlie the functional differences observed between WT and EphB3$^{-/-}$ mice after CCI injury.

3.7. EphB3 regulates D-serine but not glutamate levels after CCI injury

We had previously shown that EphB3 can regulate D-serine levels in the naïve brain (Zhuang et al., 2010), while others have shown D-serine can exacerbate excitotoxic effects of NMDA hyper-activation after injury (Katsuki et al., 2004; Shleper et al., 2005). Therefore, we analyzed transmitter levels in sham and CCI injured whole hippocampi in the presence and absence of EphB3 using a chemiluminescent assay (Fig. 7; n = 6–7/group). In the WT hippocampus during the acute CCI injury period, the D-serine levels increased at 4 and 24 h post-CCI injury (hpi) as compared with sham controls ($p = 0.0032$ and $p = 0.034$, respectively; Fig. 7A), but returned to baseline by 3 dpi and were maintained for at least 7 dpi (not shown). Examination of glutamate levels at the same time points showed no significant difference in WT CCI injured tissues compared to WT sham controls (Fig. 7B), and these basal levels were also maintained for at least 7 dpi (not shown). When we compared the level of D-serine in EphB3$^{-/-}$ shams, we observed no significant difference from WT shams. Strikingly, in the CCI injured EphB3$^{-/-}$ hippocampus, D-serine levels were not increased at 4 and 24 hpi (Fig. 7A).

Next, we examined whether ephrinB3 stimulation of Eph signaling would augment D-serine or glutamate levels in WT mice at 3 dpi, a time when transmitter levels have returned to baseline. Infusion of clustered ephrinB3-Fc (112 μg/kg/day) for 3 days into the ipsilateral hippocampus resulted in a significant increase in D-serine levels in hippocampi from WT

mice but not EphB3$^{-/-}$/EphA4$^{-/-}$ double knockout mice (Fig. 7C). EphB3$^{-/-}$/EphA4$^{-/-}$ mice where used to eliminate potential off target interactions with ephrinB3. Control anti-human-Fc molecules showed no effect on D-serine levels as compared to non-infused naïve or sham mice. Furthermore, application of clustered ephrinB3-Fc did not alter glutamate levels in either WT or EphB3$^{-/-}$/ EphA4$^{-/-}$ mice (Fig. 7D).

3.8. Increased D-serine can reverse the enhanced synaptic plasticity observed in EphB3$^{-/-}$ mice after CCI injury

To validate our conclusion that CCI injury-induced synaptic dysfunction is aggravated by EphB3 regulation of D-serine levels, we examined CA3-CA1 hippocampal fEPSPs in vivo in CCI injured EphB3$^{-/-}$ mice after vehicle or D-serine (840 μg/kg/day) infusion (Fig. 8; n = 6/group). We infused D-serine or vehicle into the contralateral ventricle for 3 days after CCI injury. EphB3$^{-/-}$ mice that received D-serine infusion demonstrated reduced basal synaptic transmission revealed by a downward shifted I/O curve at stimulation intensities of 20 μA or higher compared with vehicle-infused controls (Fig. 8A). Two-way repeated measures ANOVA showed significant interaction between groups and stimulus intensity ($p < 0.0001$), where the Bonferroni post-hoc test showed significant difference between CCI injured EphB3$^{-/-}$ vehicle-and D-serine-treated mice ($p < 0.001$). No significant differences were observed in PPF between groups (Fig. 8B); however, significant differences were observed in LTP. Specifically, we observed a significant interaction between groups and time($p < 0.0001$) and main effect for animal groups (EphB3$^{-/-}$ CCI-injured vehicle- vs. D-serine-infused; $p = 0.0087$) and time ($p < 0.0001$) (Fig. 8C). Analysis of fEPSP slope post-HFS revealed that D-serine infusion resulted in significant reductions in both early and late LTP in EphB3$^{-/-}$ CCI injured mice when compared with vehicle-infused mice ($p < 0.0001$; Fig. 8C – E). These findings support our observations that increased D-serine levels in the hippocampus are detrimental to synaptic function, and that EphB3 signaling may regulate synaptic dysfunction after CCI injury through enhanced D-serine synthesis and release.

4. Discussion

Synaptic dysfunction and impaired plasticity can have a significant impact on motor, sensory and cognitive functions in TBI patients. Neuronal cell death is a predominant underlying cause for synaptic loss in regions of tissue damage; however, synaptic dysfunction is also present in more distal brain regions where neuronal loss is not observed (Lyeth et al., 1990). To begin to examine synaptic dysfunction within the complex and evolving TBI environment, we have developed a moderate CCI injury model that leads to hippocampal synaptic damage without neuronal losses. We then examined the role of ephrins and Eph receptors in synaptic stability and function after TBI. In the CCI injured hippocampus, we found that EphB3$^{-/-}$ mice showed stable numbers of synapses compared to sham controls, and improved synaptic plasticity and learning behavior as compared with WT CCI injured mice. Comparison of key synaptic proteins essential for excitatory synaptic transmission showed no differences between WT and EphB3$^{-/-}$ mice; however, increases in the NMDAR co-agonist D-serine following CCI injury were significantly reduced in the absence of EphB3. Furthermore, rescuing D-serine levels in EphB3$^{-/-}$ mice could recapitulate the synaptic deficits observed in WT CCI injured mice. These findings suggest that elevated D-

serine levels in the hippocampus may play deleterious roles by destabilizing synapses after TBI, and are in part regulated by ephrin-EphB3 signaling.

Our observation that CCI injury results in approximately 20% synaptic losses, and >50% reduction in LTP and learning in the first week suggests that synaptic loss and dysfunction together may underlie the observed functional deficits. Our observed losses in excitatory synapses in the mouse hippocampus are less pronounced than the ~50% reduction in CA1 synapses in rats after CCI injury (Scheff et al., 2005). This discrepancy could be attributed to species-specific effects but also a higher injury severity, which also lead to CA3 pyramidal cell death. Alternatively, changes in synaptic size and morphology may also contribute to functional deficits (Carlson et al., 2015; Gao et al., 2011; Marrone et al., 2004). After injury the main difference observed was an increase in the ratio between post-SD to pre-SD area in WT mice. This could be due to spine enlargement, a reduction of presynaptic bouton size, or a combination of both. However, the opposite effect was observed in the synaptic unit of EphB3$^{-/-}$ mice after injury. When taken together with the deficits in hippocampal function observed, these findings suggest that synchronous changes in both elements of synapse morphology are important for structural stabilization and plasticity (Meyer et al., 2014). Furthermore, excess activation by increased levels of D-serine could be participating in destabilizing the synapse and causing synaptic damage (Shleper et al., 2005).

Alterations in the levels of different synaptic proteins have also been associated with deficits in synaptic plasticity after TBI (Osteen et al., 2004; Spaethling et al., 2012; Titus et al., 2013). The co-agonist binding site for D-serine is located on NR1 subunits (Johnson and Ascher, 1987; Mothet et al., 2000). Interestingly, NR1 protein levels did not change after CCI injury for either group, suggesting that increase in D-serine after injury leads to increase binding probability (Furukawa and Gouaux, 2003) and could enhance NMDA-dependent glutamatergic signaling. In the CCI injured hippocampus, we observed increased levels of the NR2B subunit of the NMDAR in bothWT and EphB3$^{-/-}$ mice, which has been shown to be associated with extra-synaptic NMDARs and the detrimental effects of NMDAR over-activation (Bading et al., 1993; Hardingham and Bading, 2010; Hardingham et al., 2002). Regulation of NMDARs after injury seems to be temporally dependent and differs between injury models (Giza et al., 2006; Hsu et al., 1998; Kumar et al., 2002; Osteen et al., 2004; Schumann et al., 2008; Small et al., 1997). In more severe models, an acute transient reduction in NR2B levels is followed by protein up-regulation at later periods (Brown et al., 2004; Kumar et al., 2002), while no difference is observed in less severe models (Giza et al., 2006; Osteen et al., 2004). Despite these discrepancies, a shift in the relative amounts of synaptic NR2A to extra-synaptic NR2B receptors has been well established to mediate damage caused by initial injury (Giza et al., 2006; Osteen et al., 2004; Small et al., 1997), and likely contributes to the CCI injury-induced deficits observed in WT mice. However, increased NR2B receptors in EphB3$^{-/-}$ mice did not result in synaptic damage or loss, suggesting that reductions in the NMDAR co-agonist D-serine likely underlie the reduced synaptic damage observed in these mice. EphB receptors have been shown to play roles in glutamate receptor activation, trafficking and localization (Antion et al., 2010; Grunwald et al., 2004; Henderson et al., 2001; Irie et al., 2005). We cannot rule out that in EphB3 deficient mice NR2B receptors may remain in the cytoplasm, are unable to become

incorporated into the extra-synaptic membranes and do not contribute to detrimental effects of over-activation.

Since our model of CCI injury did not involve hippocampal neuron loss, it suggests that neuronal excitotoxicity may be below the apoptotic threshold in the hippocampus. It is well accepted that glutamate excitotoxicity results from an acute release of glutamate from neurons within the first minutes after trauma, and leads to excessive calcium influx through over-activation of NMDARs, initiation of pro-apoptotic signaling cascades, and ultimately neuronal damage (Faden et al., 1989; Obrenovitch and Urenjak, 1997). While this likely occurs in the cortex in our model, we did not observe neuronal loss in the hippocampus even at regions directly ventral to the injury epicenter. Furthermore, there was no significant difference in total hippocampal glutamate levels at 4 h post-injury (hpi), a time-point where glutamate levels have returned to baseline (Obrenovitch and Urenjak, 1997) and the earliest time-point we tested. Conversely, the NMDAR co-agonist D-serine is up-regulated hours to days after CCI injury and contributes to synaptic damage but not cell death. Enhanced D-serine levels have also been observed in other peripheral and CNS injury models (Lin et al., 2015; Moon et al., 2015). Moreover, pharmacological reductions in D-serine levels have been shown to protect neurons from excitotoxic insult (Hama et al., 2006; Shleper et al., 2005). In the absence of EphB3, increased D-serine levels were not observed after CCI injury. This provides support to our previous gain-of-function studies showing that ephrinB3 stimulation of EphB3 could increase D-serine levels in hippocampal slices and cultured astrocytes (Zhuang et al., 2010). Excessive D-serine levels can induce synaptic damage and reverse the rescue effects associated with the absence of EphB3 after CCI injury; however, the addition of D-serine by itself was not sufficient to induce NMDA-mediated synaptic damage in hippocampal slices (Katsuki et al., 2004). Together, these findings support a role for EphB3 signaling in regulating D-serine levels as a novel mechanism by which EphB3 receptors can potentiate damage in the traumatic injured brain. Additional studies are needed to determine how these effects are mediated by EphB3 signaling and establish if D-serine release is from neurons and/or astrocytes.

TBI patients typically live with life-long cognitive impairment even in the absence of significant tissue pathology (Barth et al., 1983; Gualtieri and Cox, 1991; McAllister et al., 1999). To date, most neuroprotective strategies have focused on preserving cell survival, preventing glutamate excitotoxicity, and inhibiting secondary inflammatory responses (Beauchamp et al., 2008; Corps et al., 2015). Our findings suggest that synaptic loss and dysfunction may be an important therapeutic target. Understanding the mechanisms regulating D-serine and NMDARs contributing to the balance of synaptic stability versus dysfunction will have important neuroprotective consequences. Our study suggests Eph receptor signaling plays a role in regulating this balance, whereby inhibiting Eph receptor signaling could lead to improved synaptic numbers and function after TBI.

Supplementary Material

Refer to Web version on PubMed Central for supplementary material.

Acknowledgments

We thank Peggy Bates in the electron microscopy core facilities at the Miami Project to Cure Paralysis and Jessica Landau for assisting in our synaptic analyses. We also thank Jennifer Brazill for critical reading of the manuscript and assisting with experimental revisions, as well as Jose Mier for assistance with animal husbandry. This work was supported by the Miami Project to Cure Paralysis, NIH/NINDS NS049545 (DJL), NS30291 (DJL), F31NS089335 (EJP) and the Lois Pope Life fellowship (EJP).

References

Adams MM, Smith TD, Moga D, Gallagher M, Wang Y, Wolfe BB, Rapp PR, Morrison JH. Hippocampal dependent learning ability correlates with N-methyl-d-aspartate (NMDA) receptor levels in CA3 neurons of young and aged rats. J. Comp. Neurol. 2001; 432:230–243. [PubMed: 11241388]

Antion MD, Christie LA, Bond AM, Dalva MB, Contractor A. Ephrin-B3 regulates glutamate receptor signaling at hippocampal synapses. Mol. Cell. Neurosci. 2010; 45:378–388. [PubMed: 20678574]

Aoto J, Chen L. Bidirectional ephrin/Eph signaling in synaptic functions. Brain Res. 2007; 1184:72–80. [PubMed: 17166489]

Araque A, Carmignoto G, Haydon PG, Oliet SHR, Robitaille R, Volterra A. Gliotransmitters travel in time and space. Neuron. 2014; 81:728–739. [PubMed: 24559669]

Assis-Nascimento P, Umland O, Cepero ML, Liebl DJ. A flow cytometeric approach to analyzing endothelial cells and progenitors following traumatic brain injury. J. Neurosci. Methods. 2016; 263:57–67. [PubMed: 26854397]

Bading H, Ginty DD, Greenberg ME. Regulation of gene expression in hippocampal neurons by distinct calcium signaling pathways. Science. 1993; 260:181–186. [PubMed: 8097060]

Balu DT, Takagi S, Puhl MD, Benneyworth MA, Coyle JT. d-serine and serine racemase are localized to neurons in the adult mouse and human forebrain. Cell. Mol. Neurobiol. 2014; 34:419–435. [PubMed: 24436034]

Barth JT, Macciocchi SN, Giordani B, Rimel R, Jane JA, Boll TJ. Neuropsychological sequelae of minor head injury. Neurosurgery. 1983; 13:529–533. [PubMed: 6646380]

Beauchamp K, Mutlak H, Smith WR, Shohami E, Stahel PF. Pharmacology of traumatic brain injury: where is the “golden bullet”? Mol. Med. Camb. Mass. 2008; 14:731–740. [PubMed: 18769636]

Brody DL, Donald CM, Kessens CC, Yuede C, Parsadanian M, Spinner M, Kim E, Schwetye KE, Holtzman DM, Bayly PV. Electromagnetic controlled cortical impact device for precise, graded experimental traumatic brain injury. J. Neurotrauma. 2007; 24:657–673. [PubMed: 17439349]

Brown KM, Wrathall JR, Yasuda RP, Wolfe BB. Glutamate receptor subunit expression after spinal cord injury in young rats. Brain Res. Dev. Brain Res. 2004; 152:61–68. [PubMed: 15283995]

Burda JE, Bernstein AM, Sofroniew MV. Astrocyte roles in traumatic brain injury. Exp. Neurol. 2016; 275(Pt 3):305–315. [PubMed: 25828533]

Carlson SW, Yan H, Ma M, Li Y, Henchir J, Dixon CE. Traumatic Brain Injury Impairs Soluble N-ethylmaleimide-Sensitive Factor Attachment Protein Receptor Complex Formation and Alters Synaptic Vesicle Distribution in the Hippocampus (J. Neurotrauma). 2015

Centers for Disease Control and Prevention (CDC). CDC grand rounds: reducing severe traumatic brain injury in the United States. MMWR Morb. Mortal. Wkly Rep. 2013; 62:549–552. [PubMed: 23842444]

Chen Y, Mao H, Yang KH, Abel T, Meaney DF. A modified controlled cortical impact technique to model mild traumatic brain injury mechanics in mice. Neurotrauma. 2014; 5:100.

Corps KN, Roth TL, McGavern DB. Inflammation and neuroprotection in traumatic brain injury. JAMA Neurol. 2015; 72:355–362. [PubMed: 25599342]

DeFelipe J, Marco P, Busturia I, Merchán-Pérez A. Estimation of the number of synapses in the cerebral cortex: methodological considerations. Cereb. Cortex. 1999; 9:722–732. [PubMed: 10554995]

Edward Dixon C, Clifton GL, Lighthall JW, Yaghmai AA, Hayes RL. A controlled cortical impact model of traumatic brain injury in the rat. J. Neurosci. Methods. 1991; 39:253–262. [PubMed: 1787745]

Faden AI, Demediuk P, Panter SS, Vink R. The role of excitatory amino acids and NMDA receptors in traumatic brain injury. Science. 1989; 244:798–800. [PubMed: 2567056]

Furukawa H, Gouaux E. Mechanisms of activation, inhibition and specificity: crystal structures of the NMDA receptor NR1 ligand-binding core. EMBO J. 2003; 22:2873–2885. [PubMed: 12805203]

Gambrill AC, Barria A. NMDA receptor subunit composition controls synaptogenesis and synapse stabilization. Proc. Natl. Acad. Sci. 2011; 108:5855–5860. [PubMed: 21427228]

Gao X, Deng P, Xu ZC, Chen J. Moderate traumatic brain injury causes acute dendritic and synaptic degeneration in the hippocampal dentate gyrus. PLoS One. 2011; 6:e24566. [PubMed: 21931758]

Giza CC, Maria NSS, Hovda DA. N-methyl-d-aspartate receptor subunit changes after traumatic injury to the developing brain. J. Neurotrauma. 2006; 23:950–961. [PubMed: 16774479]

Grunwald IC, Korte M, Adelmann G, Plueck A, Kullander K, Adams RH, Frotscher M, Bonhoeffer T, Klein R. Hippocampal plasticity requires postsynaptic ephrinBs. Nat. Neurosci. 2004; 7:33–40. [PubMed: 14699416]

Gualtieri T, Cox DR. The delayed neurobehavioural sequelae of traumatic brain injury. Brain Inj. 1991; 5:219–232. [PubMed: 1933073]

Gundersen V, Storm-Mathisen J, Bergersen LH. Neuroglial transmission. Physiol. Rev. 2015; 95:695–726. [PubMed: 26084688]

Halassa MM, Fellin T, Haydon PG. The tripartite synapse: roles for gliotransmission in health and disease. Trends Mol. Med. 2007; 13:54–63. [PubMed: 17207662]

Hama Y, Katsuki H, Tochikawa Y, Suminaka C, Kume T, Akaike A. Contribution of endogenous glycine site NMDA agonists to excitotoxic retinal damage in vivo. Neurosci. Res. 2006; 56:279–285. [PubMed: 16934894]

Han H, Peng Y, Dong Z. d-serine Rescues the Deficits of Hippocampal Long-term Potentiation and Learning and Memory Induced by Sodium Fluoroacetate. Pharmacol. Biochem, Behav. 2015

Hardingham GE, Bading H. Synaptic versus extrasynaptic NMDA receptor signalling: implications for neurodegenerative disorders. Nat. Rev. Neurosci. 2010; 11:682–696. [PubMed: 20842175]

Hardingham GE, Fukunaga Y, Bading H. Extrasynaptic NMDARs oppose synaptic NMDARs by triggering CREB shut-off and cell death pathways. Nat. Neurosci. 2002; 5:405–414. [PubMed: 11953750]

Harish G, Mahadevan A, Pruthi N, Sreenivasamurthy SK, Puttamallesh VN, Keshava Prasad TS, Shankar SK, Srinivas Bharath MM. Characterization of traumatic brain injury in human brains reveals distinct cellular and molecular changes in contusion and pericontusion. J. Neurochem. 2015; 134:156–172. [PubMed: 25712633]

Henderson JT, Georgiou J, Jia Z, Robertson J, Elowe S, Roder JC, Pawson T. The receptor tyrosine kinase EphB2 regulates NMDA-dependent synaptic function. Neuron. 2001; 32:1041–1056. [PubMed: 11754836]

Henkemeyer M, Orioli D, Henderson JT, Saxton TM, Roder J, Pawson T, Klein R. Nuk controls pathfinding of commissural axons in the mammalian central nervous system. Cell. 1996; 86:35–46. [PubMed: 8689685]

Henkemeyer M, Itkis OS, Ngo M, Hickmott PW, Ethell IM. Multiple EphB receptor tyrosine kinases shape dendritic spines in the hippocampus. J. Cell Biol. 2003; 163:1313–1326. [PubMed: 14691139]

Hruska M, Henderson NT, Xia NL, Le Marchand SJ, Dalva MB. Anchoring and Synaptic Stability of PSD-95 is Driven by Ephrin-B3. Nat. Neurosci. advance online publication. 2015

Hsu JC, Zhang Y, Takagi N, Gurd JW, Wallace MC, Zhang L, Eubanks JH. Decreased expression and functionality of NMDA receptor complexes persist in the CA1, but not in the dentate gyrus after transient cerebral ischemia. J. Cereb. Blood Flow Metab. Off. J. Int. Soc. Cereb. Blood Flow Metab. 1998; 18:768–775.

Hunt DL, Castillo PE. Synaptic plasticity of NMDA receptors: mechanisms and functional implications. Curr. Opin. Neurobiol. 2012; 22:496–508. [PubMed: 22325859]

Hyder AA, Wunderlich CA, Puvanachandra P, Gururaj G, Kobusingye OC. The impact of traumatic brain injuries: a global perspective. NeuroRehabilitation. 2007; 22:341–353. [PubMed: 18162698]

Irie F, Okuno M, Pasquale EB, Yamaguchi Y. EphrinB-EphB signalling regulates clathrin-mediated endocytosis through tyrosine phosphorylation of synaptojanin 1. Nat. Cell Biol. 2005; 7:501–509. [PubMed: 15821731]

Johnson JW, Ascher P. Glycine potentiates the NMDA response in cultured mouse brain neurons. Nature. 1987; 325:529–531. [PubMed: 2433595]

Katsuki H, Nonaka M, Shirakawa H, Kume T, Akaike A. Endogenous d-serine is involved in induction of neuronal death by N-methyl-d-aspartate and simulated ischemia in rat cerebrocortical slices. J. Pharmacol. Exp. Ther. 2004; 311:836–844. [PubMed: 15240826]

Klein R. Bidirectional modulation of synaptic functions by Eph/ephrin signaling. Nat. Neurosci. 2009; 12:15–20. [PubMed: 19029886]

Kotapka MJ, Gennarelli TA, Graham DI, Adams JH, Thibault LE, Ross DT, Ford I. Selective vulnerability of hippocampal neurons in acceleration-induced experimental head injury. J. Neurotrauma. 1991; 8:247–258. [PubMed: 1803033]

Kumar A, Zou L, Yuan X, Long Y, Yang K. N-methyl-d-aspartate receptors: transient loss of NR1/NR2A/NR2B subunits after traumatic brain injury in a rodent model. J. Neurosci. Res. 2002; 67:781–786. [PubMed: 11891792]

Laird MD, Vender JR, Dhandapani KM. Opposing roles for reactive astrocytes following traumatic brain injury. Neurosignals. 2008; 16:154–164. [PubMed: 18253055]

Lin C-S, Hung S-F, Huang H-S, Ma M-C. Blockade of the N-methyl-d-aspartate glutamate receptor ameliorates lipopolysaccharide-induced renal insufficiency. PLoS One. 2015; 10:e0132204. [PubMed: 26133372]

Lowenstein DH, Thomas MJ, Smith DH, McIntosh TK. Selective vulnerability of dentate hilar neurons following traumatic brain injury: a potential mechanistic link between head trauma and disorders of the hippocampus. J. Neurosci. 1992; 12:4846–4853. [PubMed: 1464770]

Luo P, Fei F, Zhang L, Qu Y, Fei Z. The role of glutamate receptors in traumatic brain injury: implications for postsynaptic density in pathophysiology. Brain Res. Bull. 2011; 85:313–320. [PubMed: 21605633]

Luo P, Chen T, Zhao Y, Zhang L, Yang Y, Liu W, Li S, Rao W, Dai S, Yang J, et al. Postsynaptic scaffold protein Homer 1a protects against traumatic brain injury via regulating group I metabotropic glutamate receptors. Cell Death Dis. 2014; 5:e1174. [PubMed: 24722299]

Lyeth BG, Jenkins LW, Hamm RJ, Dixon CE, Phillips LL, Clifton GL, Young HF, Hayes RL. Prolonged memory impairment in the absence of hippocampal cell death following traumatic brain injury in the rat. Brain Res. 1990; 526:249–258. [PubMed: 2257484]

Marrone DF, LeBoutillier JC, Petit TL. Comparative analyses of synaptic densities during reactive synaptogenesis in the rat dentate gyrus. Brain Res. 2004; 996:19–30. [PubMed: 14670627]

Martone ME, Jones YZ, Young SJ, Ellisman MH, Zivin JA, Hu B-R. Modification of postsynaptic densities after transient cerebral ischemia: a quantitative and three-dimensional ultrastructural study. J. Neurosci. 1999; 19:1988–1997. [PubMed: 10066252]

Mayhew TM. How to count synapses unbiasedly and efficiently at the ultrastructural level: proposal for a standard sampling and counting protocol. J. Neurocytol. 1996; 25:793–804. [PubMed: 9023725]

McAllister TW, Saykin AJ, Flashman LA, Sparling MB, Johnson SC, Guerin SJ, Mamourian AC, Weaver JB, Yanofsky N. Brain activation during working memory 1 month after mild traumatic brain injury: a functional MRI study. Neurology. 1999; 53:1300–1308. [PubMed: 10522888]

Merlo L, Cimino F, Angileri FF, La Torre D, Conti A, Cardali SM, Saija A, Germanò A. Alteration in synaptic junction proteins following traumatic brain injury. J. Neurotrauma. 2014; 31:1375–1385. [PubMed: 24661152]

Meyer D, Bonhoeffer T, Scheuss V. Balance and stability of synaptic structures during synaptic plasticity. Neuron. 2014; 82:430–443. [PubMed: 24742464]

Moon J-Y, Choi S-R, Roh D-H, Yoon S-Y, Kwon S-G, Choi H-S, Kang S-Y, Han H-J, Kim H-W, Beitz AJ, et al. Spinal sigma-1 receptor activation increases the production of d-serine in astrocytes

which contributes to the development of mechanical allodynia in a mouse model of neuropathic pain. Pharmacol. Res. 2015; 100:353–364. [PubMed: 26316425]

Mothet JP, Parent AT, Wolosker H, Brady RO Jr, Linden DJ, Ferris CD, Rogawski MA, Snyder SH. d-serine is an endogenous ligand for the glycine site of the N-methyl-d-aspartate receptor. Proc. Natl. Acad. Sci. U. S. A. 2000; 97:4926–4931. [PubMed: 10781100]

Obrenovitch TP, Urenjak J. Is high extracellular glutamate the key to excitotoxicity in traumatic brain injury? J. Neurotrauma. 1997; 14:677–698. [PubMed: 9383088]

Orioli D, Henkemeyer M, Lemke G, Klein R, Pawson T. Sek4 and Nuk receptors cooperate in guidance of commissural axons and in palate formation. EMBO J. 1996; 15:6035–6049. [PubMed: 8947026]

Osier, ND., Korpon, JR., Dixon, CE. Controlled Cortical Impact Model. In: Kobeissy, FH., editor. Brain Neurotrauma: Molecular, Neuropsychological, and Rehabilitation Aspects. CRC Press/ Taylor & Francis; Boca Raton (FL): 2015.

Osteen CL, Giza CC, Hovda DA. Injury-induced alterations in N-methyl-d-aspar-tate receptor subunit composition contribute to prolonged 45calcium accumulation following lateral fluid percussion. Neuroscience. 2004; 128:305–322. [PubMed: 15350643]

Paoletti P, Bellone C, Zhou Q. NMDA receptor subunit diversity: impact on receptor properties, synaptic plasticity and disease. Nat. Rev. Neurosci. 2013; 14:383–400. [PubMed: 23686171]

Pasquale EB. Eph-ephrin bidirectional signaling in physiology and disease. Cell. 2008; 133:38–52. [PubMed: 18394988]

Peña A, Pickard JD, Stiller D, Harris NG, Schuhmann MU. Brain tissue biome-chanics in cortical contusion injury: a finite element analysis. Acta Neurochir. Suppl. 2005; 95:333–336. [PubMed: 16463876]

Perea G, Navarrete M, Araque A. Tripartite synapses: astrocytes process and control synaptic information. Trends Neurosci. 2009; 32:421–431. [PubMed: 19615761]

Rodenas-Ruano A, Perez-Pinzon MA, Green EJ, Henkemeyer M, Liebl DJ. Distinct roles for ephrinB3 in the formation and function of hippocampal synapses. Dev. Biol. 2006; 292:34–45. [PubMed: 16466709]

Saatman KE, Feeko KJ, Pape RL, Raghupathi R. Differential behavioral and his-topathological responses to graded cortical impact injury in mice. J. Neurotrauma. 2006; 23:1241–1253. [PubMed: 16928182]

Scheff, Sw, Price, Da, Hicks, Rr, Baldwin, Sa, Robinson, S., Brackney, C. Synapto-genesis in the hippocampal CA1 field following traumatic brain injury. J. Neurotrauma. 2005; 22:719–732. [PubMed: 16004576]

Schumann J, Alexandrovich GA, Biegon A, Yaka R. Inhibition of NR2B phosphor-ylation restores alterations in NMDA receptor expression and improves functional recovery following traumatic brain injury in mice. J. Neurotrauma. 2008; 25:945–957. [PubMed: 18721106]

Schwarzbach E, Bonislawski Dp, Xiong G, Cohen As. Mechanisms underlying the inability to induce area CA1 LTP in the mouse after traumatic brain injury. Hippocampus. 2006; 16:541–550. [PubMed: 16634077]

Sheng M, Kim E. The postsynaptic organization of synapses. Cold Spring Harb. Perspect. Biol. 2011; 3:a005678. [PubMed: 22046028]

Shleper M, Kartvelishvily E, Wolosker H. d-serine is the dominant endogenous coagonist for NMDA receptor neurotoxicity in organotypic hippocampal slices. J. Neurosci. 2005; 25:9413–9417. [PubMed: 16221850]

Small DL, Poulter MO, Buchan AM, Morley P. Alteration in NMDA receptor subunit mRNA expression in vulnerable and resistant regions of in vitro ischemic rat hippocampal slices. Neurosci. Lett. 1997; 232:87–90. [PubMed: 9302093]

Smith DH, Soares HD, Pierce JS, Perlman KG, Saatman KE, Meaney DF, Dixon CE, McIntosh TK. A model of parasagittal controlled cortical impact in the mouse: cognitive and histopathologic effects. J. Neurotrauma. 1995; 12:169–178. [PubMed: 7629863]

Spaethling J, Le L, Meaney DF. NMDA receptor mediated phosphorylation of GluR1 subunits contributes to the appearance of calcium-permeable AMPA receptors after mechanical stretch injury. Neurobiol. Dis. 2012; 46:646–654. [PubMed: 22426393]

Theus MH, Ricard J, Bethea JR, Liebl DJ. EphB3 limits the expansion of neural progenitor cells in the subventricular zone by regulating p53 during homeostasis and following traumatic brain injury. Stem Cells Dayt. Ohio. 2010; 28:1231–1242.

Theus MH, Ricard J, Glass SJ, Travieso LG, Liebl DJ. EphrinB3 blocks EphB3 dependence receptor functions to prevent cell death following traumatic brain injury. Cell Death Dis. 2014; 5:e1207. [PubMed: 24810043]

Titus DJ, Sakurai A, Kang Y, Furones C, Jergova S, Santos R, Sick TJ, Atkins CM. Phosphodiesterase inhibition rescues chronic cognitive deficits induced by traumatic brain injury. J. Neurosci. 2013; 33:5216–5226. [PubMed: 23516287]

Witgen BM, Lifshitz J, Smith ML, Schwarzbach E, Liang S-L, Grady MS, Cohen AS. Regional hippocampal alteration associated with cognitive deficit following experimental brain injury: a systems, network and cellular evaluation. Neuroscience. 2005; 133:1–15. [PubMed: 15893627]

Wolosker H, Blackshaw S, Snyder SH. Serine racemase: a glial enzyme synthesizing d-serine to regulate glutamate-N-methyl-d-aspartate neurotransmission. Proc. Natl. Acad. Sci. U. S. A. 1999a; 96:13409–13414. [PubMed: 10557334]

Wolosker H, Sheth KN, Takahashi M, Mothet JP, Brady RO Jr, Ferris CD, Snyder SH. Purification of serine racemase: biosynthesis of the neuromodulator d-serine. Proc. Natl. Acad. Sci. U. S. A. 1999b; 96:721–725. [PubMed: 9892700]

Xiong Y, Mahmood A, Chopp M. Animal models of traumatic brain injury. Nat. Rev. Neurosci. 2013; 14:128–142. [PubMed: 23329160]

Zhang YP, Cai J, Shields LBE, Liu N, Xu X-M, Shields CB. Traumatic brain injury using mouse models. Transl. Stroke Res. 2014; 5:454–471. [PubMed: 24493632]

Zhu Y, Liu F, Zou X, Torbey M. Comparison of unbiased estimation of neuronal number in the rat hippocampus with different staining methods. J. Neurosci. Methods. 2015; 254:73–79. [PubMed: 26238727]

Zhuang Z, Yang B, Theus MH, Sick JT, Bethea JR, Sick TJ, Liebl DJ. EphrinBs regulate d-serine synthesis and release in astrocytes. J. Neurosci. 2010; 30:16015–16024. [PubMed: 21106840]

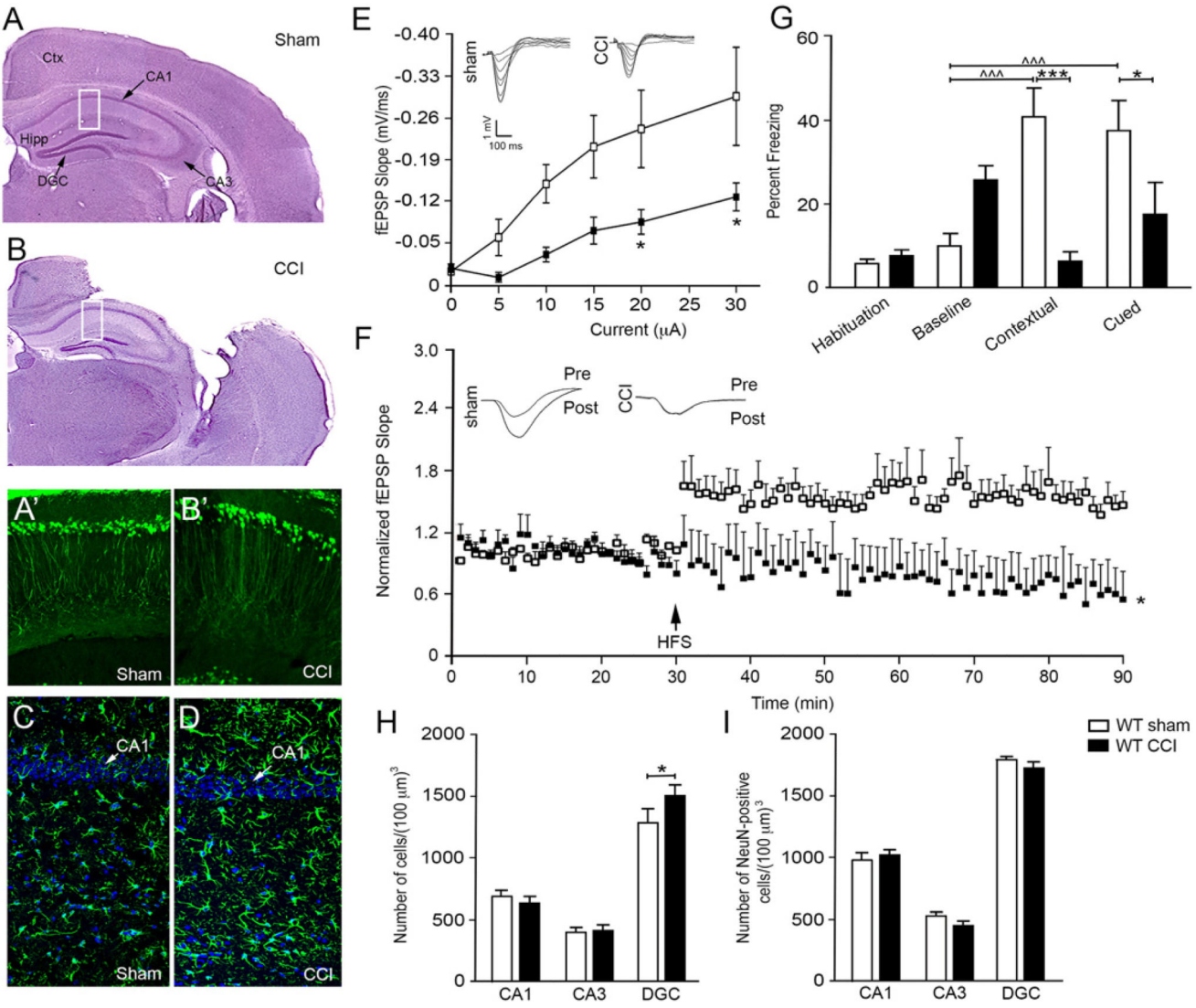

Fig. 1.

CCI injury model of synaptic dysfunction without hippocampal neuronal losses. Hematoxylin and eosin stained tissues showing gross morphological damage 7 dpi after sham (A) and CCI (B) injury. Rectangles indicate region for images in A'–B' and C–D. High magnification confocal images of CA1 pyramidal neurons in Thy-1-YFP mice show neuronal dendritic densities in sham (A') and CCI injured (B') mice. Increased astrocyte (GFAP) reactivity and hypertrophy, a hallmark of brain injury, is observed in the CA1 region of the after CCI injury (D) as compared with sham (C) mice. (E) Significant downward shift in I/O curve of fEPSPs recorded from CA1 stratum radiatum in vivo at increasing intensities of stimulation in CCI injured mice as compared with sham mice. Insets show sample fEPSP traces for I/O curve. (F) Tetanic high frequency stimulation (HFS) shows enhanced LTP in vivo in sham but not CCI injured mice, where fEPSP slopes were normalized to baseline. Inset depicts representative pre- and post-HFS traces per group. E and F, sham n = 5 and CCI injury n = 4. (G) Significant decrease in percent freezing behavior in CCI mice compared with sham mice in both contextual and cued testing (mean ± SEM; n = 7/group).

Quantitative cell counts from hematoxylin stained (H) and anti-NeuN immunoreactive (I) CA1, CA3, and DGC by non-biased stereology (n = 5/group). All data presented as mean ± SEM. *p < 0.05 and ***p < 0.001 compared with sham controls, ^^^p < 0.001 compared with habituation. Ctx, cortex; Hipp, hippocampus; CA1, CA1 pyramidal cells; CA3, CA3 pyramidal cells; DGC, dentate granule cells.

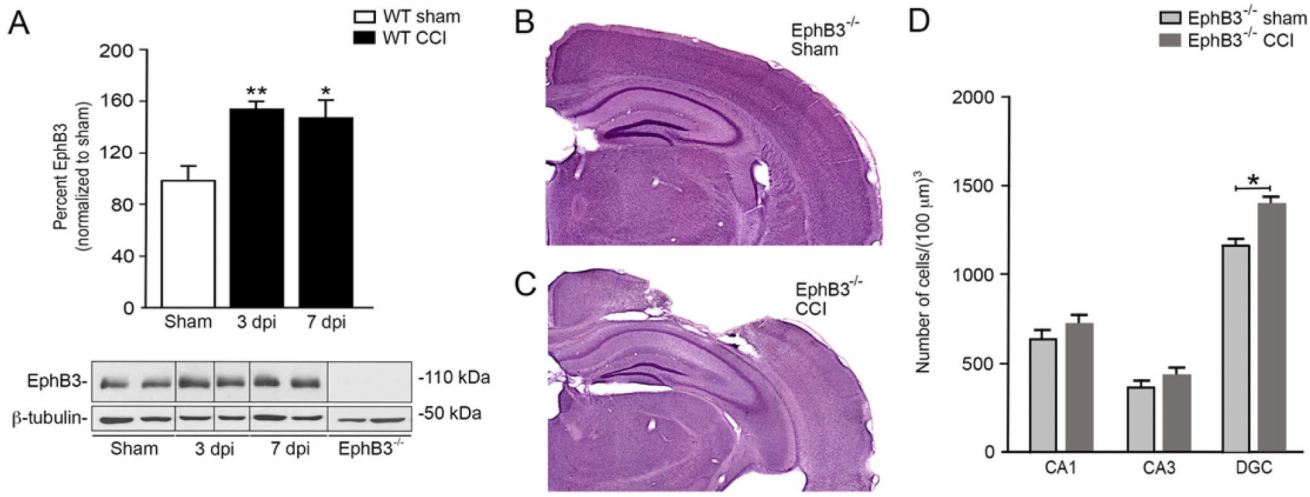

Fig. 2.

Increased levels of EphB3 does not affect cell survival in the hippocampus after CCI injury. (A) Western blots show increased hippocampal EphB3 protein levels at 3 and 7 dpi in WT mice, which were standardized to β-tubulin and normalized to sham (mean ± SEM; n = 4/group, repeated in triplicate). For full blots see SFig. 4. Hematoxylin and eosin stained EphB3$^{-/-}$ sham (B) and CCI (C) injured tissue showing gross morphological damage. (D) Number of hippocampal cells within each region in EphB3$^{-/-}$ sham and CCI injured mice (mean ± SEM; n = 5/group). *p < 0.05 and **p < 0.01.

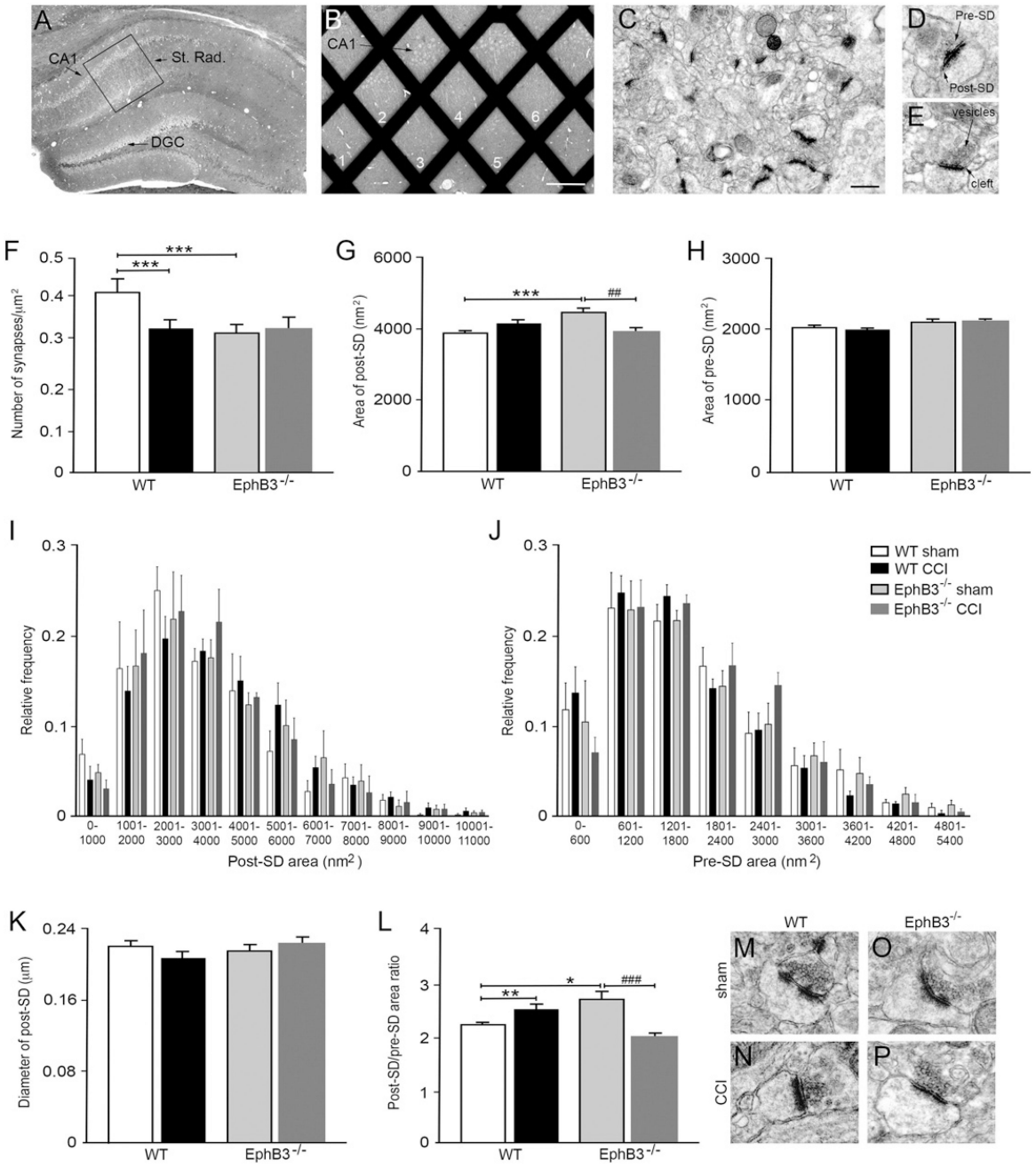

Fig. 3.

CCI injury leads to EphB3-dependent synaptic loss and alterations in pre- and post-synaptic densities in the hippocampus. (A) Cresyl violet stain of hippocampal tissue, where box indicates region within CA1 stratum radiatum selected for sectioning and grid placement. (B) Grid numbers represent random sampling fields for image acquisition (scale bar = 500 µM). (C) Representative 25,000× electron micrograph of CA1 stratum radiatum with EPTA-stained excitatory synapses (scale bar = 50 µM). High magnification images of synapses with asymmetrical pre- and post-SDs (D) and clear, delineated synaptic cleft and pre-synaptic vesicles (E). (F) CCI injury resulted in a reduction in synaptic numbers in WT, but

not EphB3$^{-/-}$ when compared with sham controls. (G) Quantification of mean post-SD area showed EphB3$^{-/-}$ shams had increased post-SD area when compared with both WT sham and EphB3$^{-/-}$ CCI group. (H) Quantification of mean pre-SD area showed no difference between groups. Frequency distribution plots show positively-skewed curve of post-SD area (I) and pre-SD area (J). (K) Quantification of mean post-SD diameter showed no significant differences between groups. (L) Comparison of the ratio between post-SD to pre-SD areas showed opposing CCI injury-induced effects in WT and EphB3$^{-/-}$ mice, where CCI lead to an increase in WT ratio and decrease in EphB3$^{-/-}$ ratio. (M–P) Representative synapses for each group reflect changes observed in synaptic quantifications. All data presented as mean ± SEM with n = 4/group with at least 20 micrographs per animal. *$p < 0.05$, **$p < 0.01$, ***$p < 0.001$ compared with WT sham, and $^{\#\#}p < 0.01$; $^{\#\#\#}p < 0.001$ compared with EphB3$^{-/-}$ sham.

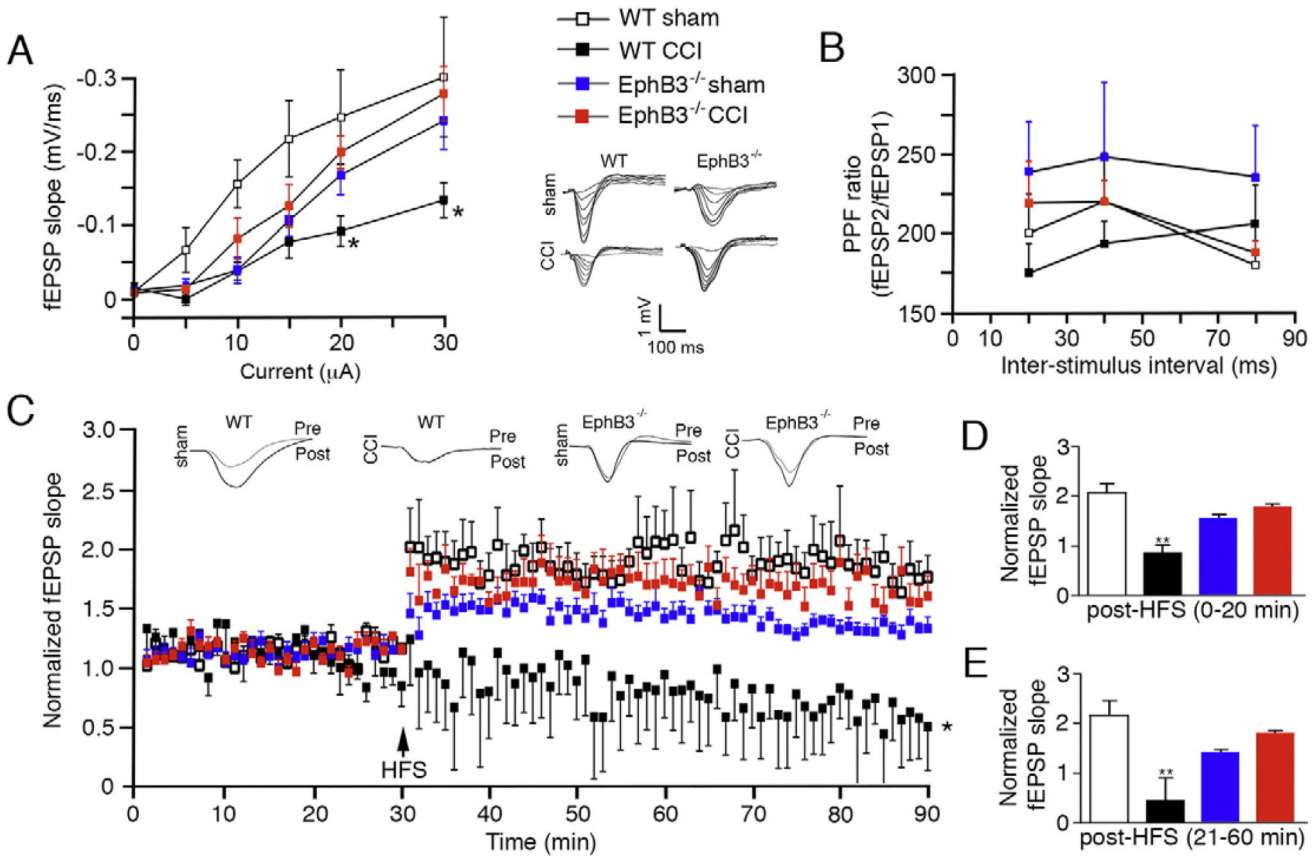

Fig. 4.

Synaptic plasticity is significantly reduced in the hippocampus at 7 dpi in WT but not EphB3$^{-/-}$ mice. (A) I/O curve plotting the in vivo hippocampal fEPSP at increasing stimulus intensities shows CCI injury in WT mice resulted in a significant downward shift at higher stimulus intensities, while no significant difference was observed in the EphB3$^{-/-}$ CCI group when compared to EphB3$^{-/-}$ sham group. Inset, superimposed representative traces of evoked fEPSPs at increasing current intensities. (B) Examination of PPF, the ratio of second fEPSP to the first fEPSP slope, revealed no significant differences between animal groups. (C) Examination of LTP, normalized to baseline fEPSP slope, in vivo at the CA1 hippocampal synapse showed significant CCI injury-induced deficit in WT but not EphB3$^{-/-}$ mice. Analysis of fEPSP slope post-HFS revealed that injury resulted in significant reductions in both early (D) and late (E) phase LTP in WT CCI mice when compared with WT sham mice. No differences were observed between EphB3$^{-/-}$ sham and EphB3$^{-/-}$ CCI-injured mice for either early or late LTP responses. All data presented as mean ± SEM. WT sham, n = 5; WT CCI, n = 4; EphB3$^{-/-}$ sham, n = 6; EphB3$^{-/-}$ CCI, n = 5. *p < 0.05, **p < 0.01 compared with WT sham.

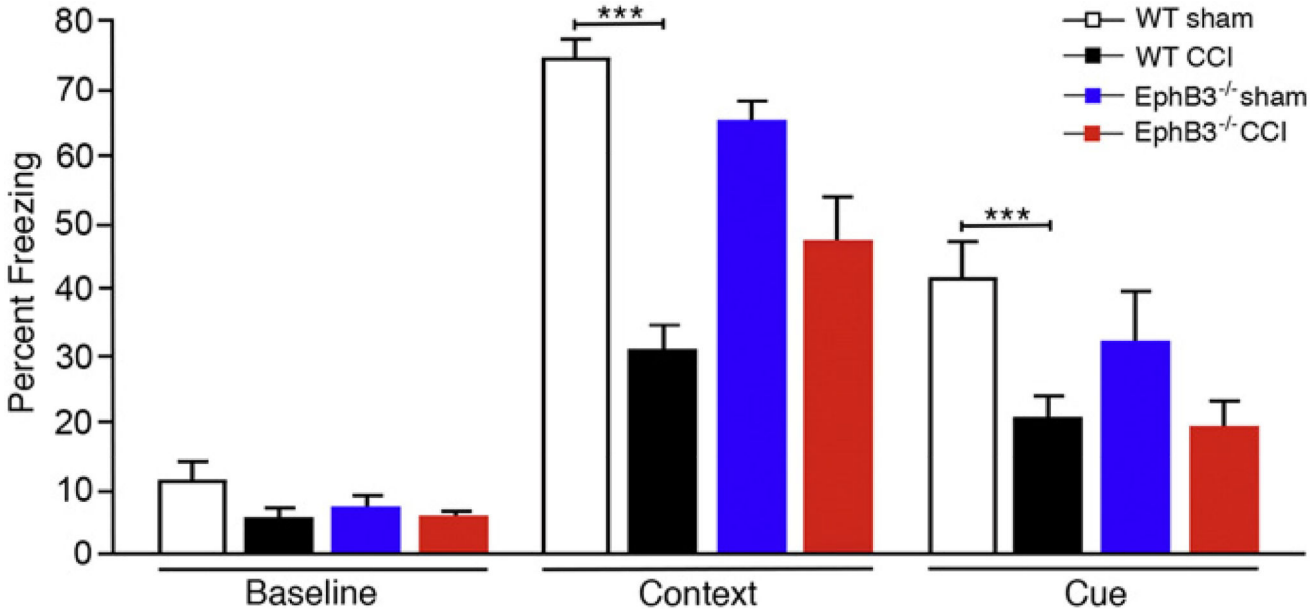

Fig. 5.

Hippocampal learning is significantly reduced at 7 dpi in WT but not EphB3$^{-/-}$ mice. Hippocampal-dependent fear-conditioning behavior quantified as percent freezing showed no significant differences between sham and CCI and between genotypes at baseline; however, a significant decrease in freezing behavior in both contextual and cued learning was observed in WT CCI mice when compared with WT sham mice. Nonsignificant reductions were observed in EphB3$^{-/-}$ CCI injured mice compared to EphB3$^{-/-}$ sham mice in both contextual and cued learning. Data presented as mean ± SEM. WT sham, n = 10; WT CCI, n = 15; EphB3$^{-/-}$ sham, n = 10; EphB3$^{-/-}$ CCI, n = 8. ***$p < 0.001$ compared with WT sham.

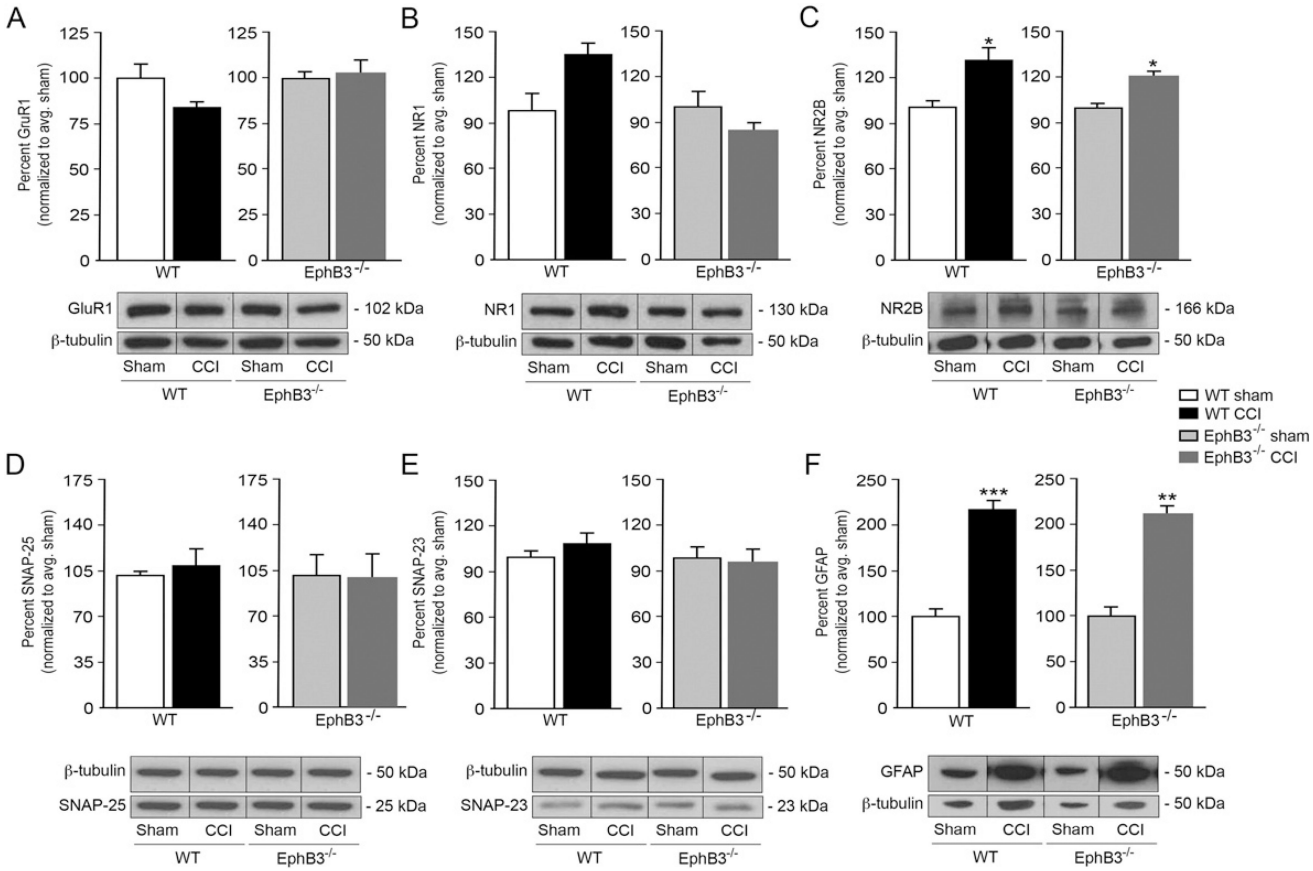

Fig. 6.

CCI-induced alterations in synaptic protein levels are similar in WT and EphB3$^{-/-}$ hippocampi at 7 dpi. CCI injury did not result in significant changes in levels of GluR1 (A), NR1 (B), SNAP-25 (D) and SNAP-23 (E), but NR2B (C) was upregulated in both WT and EphB3$^{-/-}$ mice. (F) GFAP, a marker of reactive astrocytosis, was significantly upregulated after CCI with no differences between WT and EphB3$^{-/-}$ CCI groups. Insets, representative Western blots for each protein, including beta-tubulin as a loading control. For full blots see SFig. 4. All data presented as mean ± SEM; n = 4/group, repeated in triplicate. *$p < 0.05$, **$p < 0.01$, ***$p < 0.001$ compared with sham control.

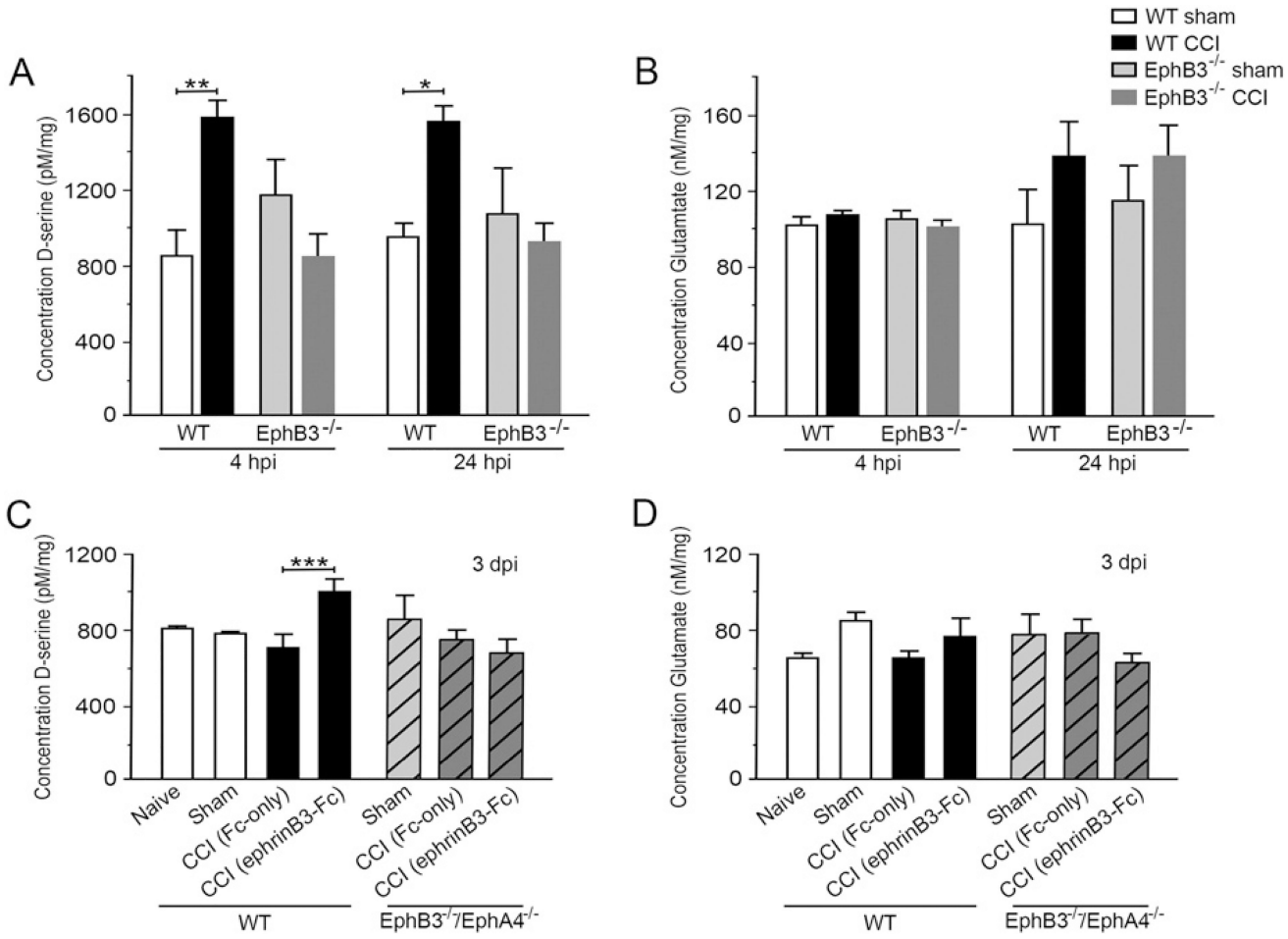

Fig. 7.

Eph receptor signaling regulates injury-induced changes in D-serine but not glutamate levels in the hippocampus. CCI injury lead to significant increases in total levels of D-serine in WT but not EphB3$^{-/-}$ hippocampi at 4 and 24 hpi (A), while no significant changes were observed in total glutamate levels (B) at these time points. EphrinB3 stimulation of Eph signaling lead to increased levels of D-serine in WT but not EphB3$^{-/-}$/EphA4$^{-/-}$ mice at 3 dpi (C), while having no effect on levels of glutamate in both groups of mice (D). All data presented as mean ± SEM; A, n = 7/group; B, n = 6/group; C, n = 7/group; D, n = 6/group. *$p < 0.05$, **$p < 0.01$, ***$p < 0.001$ compared with WT sham.

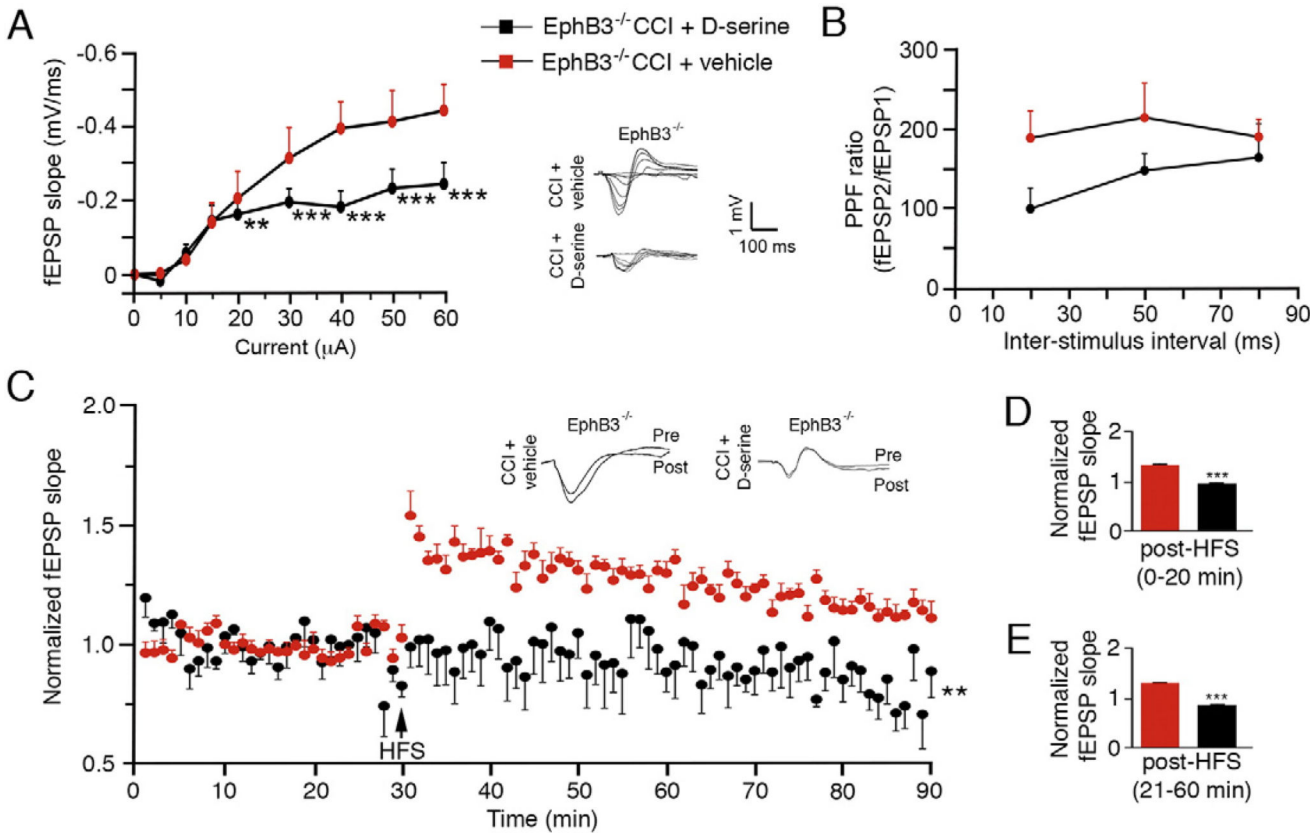

Fig. 8.

Infusion of D-serine can reverse the enhanced synaptic plasticity observed in EphB3$^{-/-}$ mice at 7 dpi. (A) Basal synaptic transmission is diminished after D-serine but not vehicle infusion in EphB3$^{-/-}$ mice, as seen by downward shift in I/O curve in current intensities of 20 mA or higher. Inset, superimposed representative traces of evoked fEPSPs at increasing current intensities. (B) Examination of presynaptic function through PPF revealed no significant differences between animal groups. (C–E) A significant reduction in LTP was observed in D-serine- versus vehicle-treated EphB3$^{-/-}$ mice. Examination of LTP in vivo at the CA1 hippocampal synapse showed a significant injury-induced deficit in D-serine but not vehicle-infused EphB3$^{-/-}$ mice (C). Analysis of fEPSP slope post-HFS revealed that injury resulted in significant reductions in both early (D) and late (E) phase LTP in D-serine infused EphB3$^{-/-}$ mice when compared with vehicle-infused EphB3$^{-/-}$ mice. All data presented as mean ± SEM; EphB3$^{-/-}$ CCI + vehicle, n = 6; EphB3$^{-/-}$ CCI + D-serine, n = 6. **p < 0.01, ***p < 0.001 compared with vehicle-infused group.